

Confinement of Bloch surface waves in a graphene-based one-dimensional photonic crystal and sensing applications

Xiu-Juan Zou(邹秀娟), Gai-Ge Zheng(郑改革), Yun-Yun Chen(陈云云)
Citation: Chin. Phys. B . 2018, 27(5): 054102. **doi:** 10.1088/1674-1056/27/5/054102

Journal homepage: http://cpb.iphy.ac.cn; http://iopscience.iop.org/cpb

What follows is a list of articles you may be interested in

Design of scale model of plate-shaped absorber in a wide frequency range

Li-Ming Yuan(袁黎明), Yong-Gang Xu(许勇刚), Wei Gao(高伟), Fei Dai(戴飞), Qi-Lin Wu(吴琪琳)
Chin. Phys. B . 2018, 27(4): 044101. **doi:** 10.1088/1674-1056/27/4/044101

A broadband cross-polarization conversion anisotropic metasurface based on multiple plasmon resonances

M Ismail Khan, Farooq A Tahir
Chin. Phys. B . 2018, 27(1): 014101. **doi:** 10.1088/1674-1056/27/1/014101

An electrically tunable metasurface integrated with graphene for mid-infrared light modulation

Zongpeng Wang(王宗鹏), Ya Deng(邓娅), LianFeng Sun(孙连峰)
Chin. Phys. B . 2017, 26(11): 114101. **doi:** 10.1088/1674-1056/26/11/114101

Ultra-broadband and polarization-independent planar absorber based on multilayered graphene

Jiao Wang(王娇), Chao-Ning Gao(高超宁), Yan-Nan Jiang(姜彦南), Charles Nwakanma Akwuruoha
Chin. Phys. B . 2017, 26(11): 114102. **doi:** 10.1088/1674-1056/26/11/114102

Tunable coupling of a hybrid plasmonic waveguide consisting of two identical dielectric cylinders and a silver film

Benli Wang(王本立), Han Liang(梁涵), Jiafang Li(李家方)
Chin. Phys. B . 2017, 26(11): 114103. **doi:** 10.1088/1674-1056/26/11/114103

Confinement of Bloch surface waves in a graphene-based one-dimensional photonic crystal and sensing applications*

Xiu-Juan Zou(邹秀娟)[1,2], Gai-Ge Zheng(郑改革) [1,2,3,†], and Yun-Yun Chen(陈云云) [1,2,3]

[1] *Jiangsu Key Laboratory for Optoelectronic Detection of Atmosphere and Ocean, Nanjing University of Information Science & Technology, Nanjing* 210044, *China*

[2] *School of Physics and Optoelectronic Engineering, Nanjing University of Information Science & Technology, Nanjing* 210044, *China*

[3] *Jiangsu Collaborative Innovation Center on Atmospheric Environment and Equipment Technology (CICAEET), Nanjing University of Information Science & Technology, Nanjing* 210044, *China*

(Received 1 December 2017; revised manuscript received 10 January 2018; published online 26 April 2018)

Bloch surface waves (BSWs) are excited in one-dimensional photonic crystals (PhCs) terminated by a graphene monolayer under the Kretschmann configuration. The field distribution and reflectance spectra are numerically calculated by the transverse magnetic method under transfer-matrix polarization, while the sensitivity is analyzed and compared with those of the surface plasmon resonance sensing method. It is found that the intensity of magnetic field is considerably enhanced in the region of the terminated layer of the multilayer stacks, and that BSW resonance appears only in the interface of the graphene and solution. Influences of the graphene layers and the thickness of a unit cell in PhCs on the reflectance are studied as well. In particular, by analyzing the performance of BSW sensors with the graphene monolayer, the wavelength sensitivity of the proposed sensor is 1040 nm/RIU whereas the angular sensitivity is 25.1°/RIU. In addition, the maximum of figure of merit can reach as high as 3000 RIU^{-1}. Thus, by integrating graphene in a simple Kretschmann structure, one can obtain an enhancement of the light–graphene interaction, which is prospective for creating label-free, low-cost and high-sensitivity optical biosensors.

Keywords: optical sensor, Bloch surface wave (BSW), photonic crystal (PhC)

PACS: 41.20.jb, 78.67.pt **DOI:** 10.1088/1674-1056/27/5/054102

1. Introduction

The spectroscopy of attenuated total reflection (ATR) has been applied widely in chemical and biological sensors. Optical sensors based on surface waves (SWs) excited under the ATR condition,[1] which are electromagnetic (EM) waves that propagate along the interface of two different media and can be confined strongly at the interface, have become powerful diagnostic tools due to their unique properties, such as high surface sensitivity,[2] real-time and label-free detection.[3] The most common SW, which is widely used in the sensing design, is undoubtedly surface plasmon resonance (SPR).[4,5] Surface plasmon polaritons (SPPs) are collective oscillations of charge density at the interface between a metal and a dielectric layer. High angular and wavelength sensitivity have been attained in popular SPR sensors.[6,7] Bloch surface waves (BSWs) are EM modes confined at the interface of a homogeneous medium and a finite 1D photonic crystal (PhC),[8–10] have been proposed as an alternative to SPR.[11–14] BSW sensors have some similar characteristics with those of SPR but bear some distinctly different features.[15,16] The use of BSWs is more flexible and efficient than the use of SPR. This is due to the fact that SWs in dielectric media can be absorption-free. In addition, the BSW dispersion relation can be easily engineered, providing long-range guiding properties and being inherently inert with respect to sensitive biological materials to optimize device performance.[17–20]

In recent years, graphene's unique optical and electronic properties including the strong light–graphene interaction and the broadband high-speed operation have attracted intense scientific interest.[21–26] Graphene is used as a sensing material due to its high specific surface area and unique electrical properties such as high mobility and low electrical noise. Graphene promises a variety of exciting applications for conventional plasmonics, attributed to its intrinsic plasmons that are tunable and adjustable.[27] It has been proved to be a suitable alternative to the conventional noble metals due to the ability of dynamically tuning its SP spectrum by chemical and electrical doping in real time locally and in homogeneously.[28] Thus, graphene is promising in overcoming the problem of poor confinement of SW in sensing applications.

In this context, here we propose a graphene-based 1D PhC and demonstrate the excitation of surface EM waves in the multilayer at optical frequencies under the Kretschmann configuration. The effects of the thickness of the PhCs and the graphene layers on the magnitude and location of the reflection dip caused by the BSW resonance are investigated. The proposed graphene-based 1D periodic structure has low loss, which gives a narrow reflectivity resonance and high sur-

*Project supported by the National Natural Science Foundation of China (Grant Nos. 61203211 and 41675154), the Six Major Talent Peak Expert of Jiangsu Province, China (Grant No. 2015-XXRJ-014), and the Natural Science Foundation of Jiangsu Province, China (Grant No. BK20141483).

†Corresponding author. E-mail: jsnanophotonics@yahoo.com

© 2018 Chinese Physical Society and IOP Publishing Ltd

face fields. It is also found that the incident angle plays a fundamental role in the magnitude of resonance wavelength and reflectance simultaneously. Finally, the effect of the small refractive index (RI) variations of the bio-solution on the sensitivity of the proposed structure is analyzed and discussed.

2. Theoretical background and model

Figure 1 shows the typical Kretschmann prism-coupled sample structure schematically. It consists of a repeating multilayer of two nonmagnetic dielectric materials and graphene nanolayers are tightly attached to the top of the 1D PhC. The thickness of graphene monolayer is 0.34 nm, and its RI can be expressed by $n_g = 3 + \mathrm{j}5.446\lambda/3$ (where λ is the operating wavelength with a unit of micrometers).[29–31] Graphene's complex RI can effectively describe the optical behavior to the bulk limit, as reported in Ref. [30]. The RI of the standard input prism is set as 1.51 which is close to that of the BK7 glass in the near-infrared range. In each unit of the PhCs, we choose Ta_2O_5 (RI $n_H = 2.1$) as the high RI material and SiO_2 ($n_L = 1.46$) as the low RI material. To see the details of the structure more clearly and to facilitate the following calculation, one unit of the periodic part is presented in Fig.1(b). Their thicknesses are 148 nm (Ta_2O_5) and 260 nm (SiO_2), respectively. The total number of the unit cells is defined as T, and the optimized parameter T is set to be 18. Due to the characteristics of graphene that it behaves like a thin metal in TM polarization when imaginary part of the graphene conductivity is negative, the incident light is chosen to be incident at an angle of θ.[32] There has already been an investigation on the Kretschmann configuration containing 1D PhCs and a metal layer for the optical sensor.[33] Advantages of this BSW approach in contrast to SPR are that the BSW dispersion can be almost arbitrarily tuned by the stack design and the layer materials used, which means that the BSW can operate at any wavelength and the resonance angle can also be adjusted to maximum sensitivity. In the present study, we present an alternative approach to excite BSW with graphene-terminated 1D PhCs. Meanwhile, the designed sensor with confinement of BSWs is expected to acquire a characteristic of high sensitivity so that it can have extensive applications in optical sensors.

In the investigation of the performance of the BSW sensor, the reflectance, sensitivity, field distribution as well as figure of merit (FOM) are analyzed through the transfer-matrix method (TMM).[34,35] The EM fields of the transfer-matrix polarized wave ($H_x = H_z = 0$, $E_y = 0$) in each layer (j) can be described as

$$\begin{cases} H_{yj}(x,z) = H_{yj}(z)\,\mathrm{e}^{-\mathrm{i}k_x x} = (A_j\,\mathrm{e}^{\mathrm{i}k_{j,z}z} + B_j\,\mathrm{e}^{-\mathrm{i}k_{j,z}z})\,\mathrm{e}^{-\mathrm{i}k_x x}, \\ E_{xj}(x,z) = \dfrac{\mathrm{i}k_x}{\omega\varepsilon} H_{yj}(x,z), \\ E_{zj}(x,z) = \dfrac{-\mathrm{i}}{\omega\varepsilon}\dfrac{\mathrm{d}H_{yj}(x,z)}{\mathrm{d}z}, \end{cases} \tag{1}$$

where $k_{j,z} = \sqrt{(\frac{\omega}{c})^2\varepsilon_j - k_x^2}$ is the wave number, and the TM mode is defined as the component of the magnetic field parallel to the surface of the 1D PhCs. j indicates layers of high RI material (H) and low RI material (L) with electric permittivity ε_j and magnetic permeability μ_j, respectively. The transverse wave vector component, $k_x = k_0 \sin\theta$, is preserved across all interface. Also, for the bio-solution, $k_s = -\mathrm{i}\sqrt{(\frac{\omega}{c})^2\varepsilon_s - k_x^2}$.[35] The propagation matrix that propagates freely through a given material is given by

$$p_j = \begin{pmatrix} \exp(-\mathrm{i}k_{j,z}d_j) & 0 \\ 0 & \exp(\mathrm{i}k_{j,z}d_j) \end{pmatrix}. \tag{2}$$

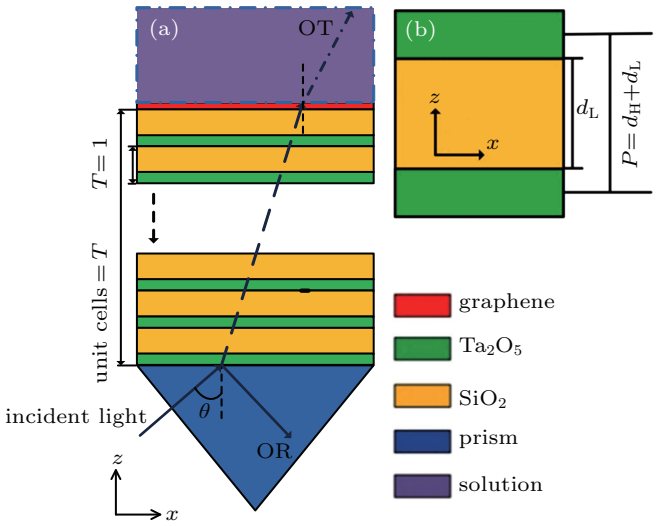


Fig. 1. (color online) (a) Schematic diagram of the sensor design, which consists of a prism, 1D PhCs, a graphene monolayer and the bio-solution to be estimated. The incident light is incident at an angle of θ with TM polarization. (b) A more detailed view of a unit cell. The thickness of a unit cell is P.

The dynamic matrix that propagates through the boundary of two dielectrics is defined as

$$D_{j,j+1} = \frac{1}{2}\begin{pmatrix} 1+c & 1-c \\ 1-c & 1+c \end{pmatrix}, \quad c = \frac{k_{j+1,z}\varepsilon_{j,z}}{k_{j,z}\varepsilon_{j+1,z}}. \tag{3}$$

When the total number of medium layers is J, the transfer matrix M of the whole medium is given by

$$M = D_{0,1}P_1D_{1,2}\cdots P_{J-1}D_{J-1,J}. \tag{4}$$

We can relate the field of the top layer to that of the bottom layer as

$$\begin{pmatrix} A_{\mathrm{prism}} \\ B_{\mathrm{prism}} \end{pmatrix} = M\begin{pmatrix} A_{\mathrm{solution}} \\ B_{\mathrm{solution}} \end{pmatrix}, \quad M = \begin{pmatrix} M_{11} & M_{12} \\ M_{21} & M_{22} \end{pmatrix}, \tag{5}$$

where M is the total transfer matrix that relates the field coefficients (A, B) of the first layer to the ones of the last layer of the whole structure.[36,37] The reflectance of the structure is given by

$$R = \left|\frac{M_{21}}{M_{11}}\right|^2. \tag{6}$$

3. Results and discussions

The Kretschmann configuration is a great technique for exciting SWs.[38] In this configuration, by using an appropriate prism, light is coupled to the non-radiative SW. The excitation of SWs can be achieved by a dip appearing in the reflection spectrum. The dip location depends on the RI of biomolecules that are immobilized at the interface between the sensor and the fluid in which an analyte exists. The localization of the BSW at the interface between graphene monolayer and an external dielectric medium, generally an aqueous solution, can be guaranteed by Bragg reflection and ATR on the two sides of the interface. Firstly, we calculate the reflection spectrum of the proposed BSW sensor structure based on the parameters given above, as shown in Fig. 2. It is evident that the obtained resonance wavelength is 713.03 nm, this deepest dip corresponds to the non-radiative SWs propagating at the graphene/binding layer boundary. The only narrow reflection dip appears in the whole visible and near-infrared wavelength regions, indicating good wavelength selectivity. The proposed biosensor configuration provides a deeper, narrower dip as compared to the SPR biosensor. It is evident that the graphene-based 1D PhC has low loss and maximal surface mode excitation compared to the SPR biosensor.

The field distribution at the sensing layer interface largely affects the overall performance of the BSW sensor through the overlap integral between the evanescent field and the spatial distribution of the dielectric constant of the sensing region. The field distributions and the magnitude as a function of thickness along $+Z$ direction are simulated. Figure 3(a) illustrates the 2D plot of magnetic field intensity ($|H_y|$) distribution with distance normal to the interface. Such high magnetic field at the graphene–sensing layer interface has a corresponding high electric field intensity and in turn can help to achieve the high performance of graphene-based BSW sensors. Note that the output magnetic field is normalized with respect to the incident field. Figure 3(b) shows the 1D plot of the absolute value of magnetic field intensity ($|H_y|$) parallel to the interface as a function of distance normal to the interface for sensing layer RI of 1.330 and operating wavelength 713 nm. It is visible that the intensity decays toward the prism/1D PhC interface and the field oscillates many times throughout the periodic structure. One can obviously count out that there are 18 peaks in the region of 1D PhCs. The positions of peaks are located in the L–H interface (i.e., the interface from low RI dielectric to high RI dielectric) and the positions of dips located in the H–L interface. According to Fig. 3(b), it is also clear that when the surface mode is excited, the EM field enhancement occurs within the last layer of the 1D PhC. The maximal field enhancement factor is observed at graphene/binding layer interface, which is due to the tighter confinement mode to the surface.[39] The magnetic field intensity in the bio-solution is gradually decaying along the $+Z$ direction, explaining that the interaction between light and solution declines with the increasing distance away from the truncated layer. It also shows that the mode at the band edge has less attenuation and thus the decaying evanescent filed can penetrate much further into the 1D PhC.

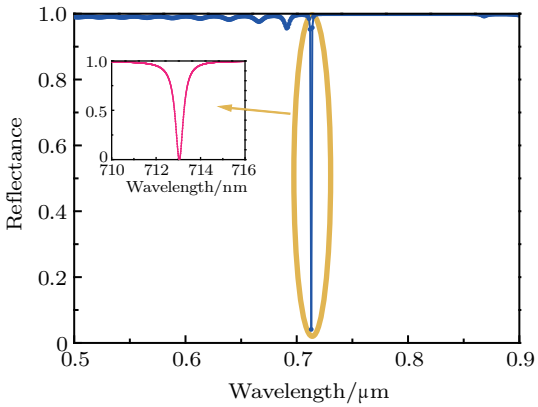


Fig. 2. (color online) Reflection spectrum of the proposed sensor with the parameters given above with $\theta = 63°$. Inset: amplification of the reflection dip with a resolution of wavelength reaching 0.01 nm.

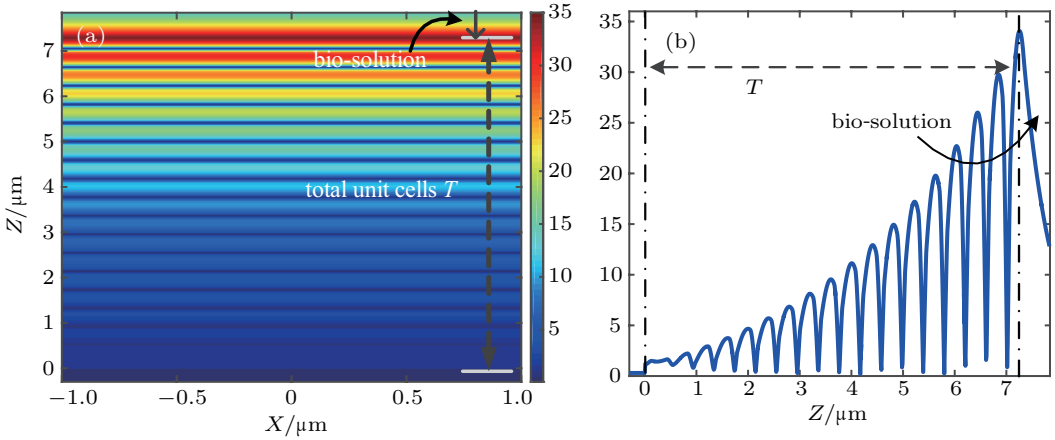


Fig. 3. (color online) (a) Density plot of the magnetic field distribution in the 2D plane of the proposed structure at $\lambda = 713$ nm under TM polarization. (b) Magnitude of magnetic field as a function of thickness along the $+Z$ direction. The parameters are chosen as $T = 18$, $d_H = 0.148$ μm, $d_L = 0.26$ μm, $\theta = 63°$.

By the proper design of the multilayer stack, the performances of the resonance in terms of dispersion as well as resonance width, depth and shift can be adapted. A periodic high (H)/low (L) reflector is taken because the light inside the stack has to be optimally reflected to achieve the resonant mode with the light that is totally reflected at the upper boundary. To reveal the physical mechanism of the unity absorption of the graphene monolayer and the ultra-narrowband response of the designed graphene sensor, the resonance spectrum of the sensor is plotted as a function of wavelength for variable thicknesses of one unit cell in the 1D PhCs, as shown in Fig. 4. When d_{H} changes from 0.1 to 0.2 μm (Fig. 4(a)) and d_{L} varies between 0.2 and 0.3 μm (Fig. 4(b)), the reflection dips of the BSW resonance are red-shifted in both cases. Furthermore, the locations of reflection dips are related to the thicknesses of the two dielectric materials linearly. It can be seen that the slope related to d_{L} is larger than d_{H}. In other words, the increase of d_{L} causes a larger red-shift of resonant wavelength than that of d_{H}. Thus, we can first change the thickness of SiO_2 to adjust the resonant wavelength, and then alter the thickness of Ta_2O_5 to fine-tune the resonant wavelength to minimize the reflectivity of the BSW resonance.

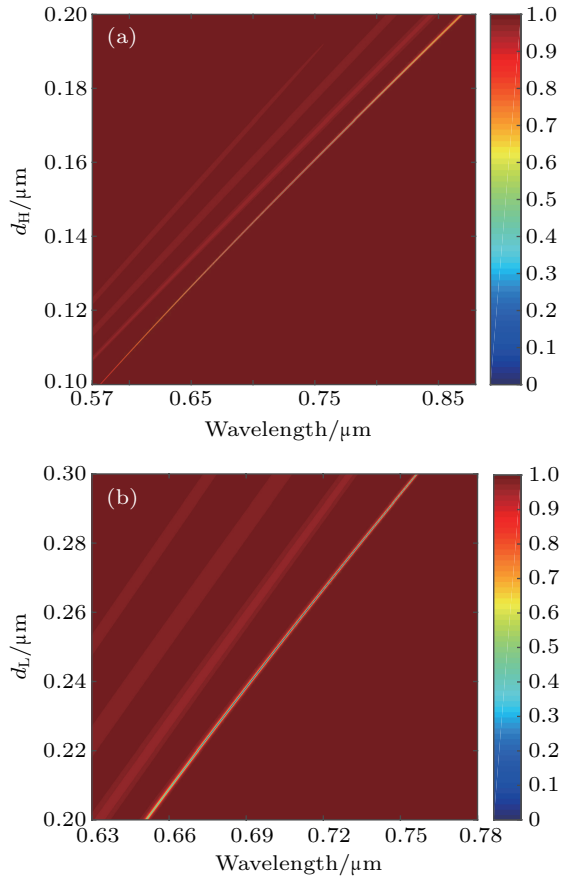


Fig. 4. (color online) (a) Density plots of the reflectance of the sensing structure as a function of wavelength with a variation of the thickness of Ta_2O_5 (d_{H}) with the thickness of SiO_2 (d_{L}) maintains 0.26 μm. (b) Density plots of the reflectance with a variation of d_{L} and $d_{\mathrm{H}} = 0.148$ μm. Spectra are calculated for $\theta = 63^\circ$ and the other parameters are kept unchanged.

In order to comprehensively consider the factors which affect the reflection dip, the influence of the number of graphene layers on absorption enhancement is also investigated and plotted in Fig. 5. It shows that the graphene-based 1D PhC has low loss and maximum surface mode excitation compared to the SPR biosensor.[19] It is found that the minimum (value of near-zero) of the reflective resonance related to the BSW is observed when the graphene monolayer is introduced and there is a little red-shift in the BSW mode resonance with the increase of the graphene layers. It can be seen that the reflectance of the sensor structure without graphene in the whole wavelength region remains a constant, demonstrating the role of the graphene layer in exciting BSW resonance.[40] The reflection dip of the BSW sensor is gradually reduced and the FWHM (full width at half minima) is widened, indicating that the sensitivity declines with the increase in the number of graphene layers. The increase in FWHM with graphene layers is due to the finite imaginary part of the dielectric constant of graphene. The BSW curve broadens for a higher number of graphene layers, as the concentration of SWs inside graphene multilayer increases due to their increased penetration depth resulting from increased in-plane wave vector. Hence, SWs exhibit damped oscillation and the FWHM is a linear function of damping, so the FWHM increases with increasing the number of graphene monolayer which leads to wider curves.

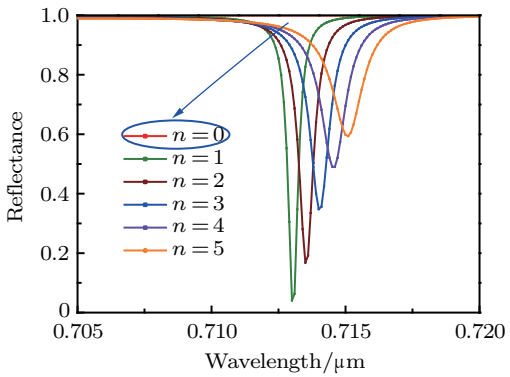


Fig. 5. (color online) Shift of spectral curves of reflectivity as a function of wavelength with increasing number of graphene layers. All the other parameters are consistent with that in Fig. 2.

In the application of graphene-based photonic devices, the proposed device structures should ensure high optical absorption efficiency working over a wide range of incident angles. To achieve a deeper understanding of the reflection dip of the sensor based on BSW resonance, the relationship between angle and wavelength is analyzed in Fig. 6. The angles shown are those inside the prism, calculated from the external angle in the air by using Snell's law. The angle variation is in the range of 62°–68°, because the BSW resonance can hardly be excited in the range of the rest angles. The absorption of graphene is significantly enhanced by appropriately choosing the incident angle. The total absorption resonance can be ob-

tained within an angle range of 62°–64°. The increasing angle leads to the blue-shift of the locations of resonance in the visible range, clearly indicating the way of designing sensor geometries to get the best performance of sense. It is also observed that the resonance intensity of the reflectivity obtains a near-zero value in a very small range of angles. Thus, it is expected that high sensitivity of graphene-based 1D PhCs biosensor can be achieved.

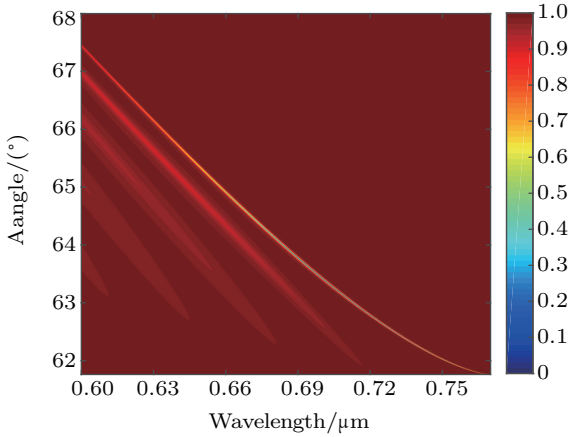


Fig. 6. (color online) Density plots of the reflectance of the BSW-based optical sensor as the functions of the incident angle varied from 62° to 68° and the incident light wavelength at the region of 0.60–0.77 μm. It is calculated by the proposed structure with TM polarization.

Due to the high field intensity associated with the state at the graphene/solution interface, this structure may have potential use as a sensor. In addition to optimizing the structural parameters of the sensor, which is conducive to the fabrication process, we also carry out an evaluation of the performance of the sensor. The sensitivity (S) of the sensor plays an important role in characterizing the sensing performance. It is a response to the variation of the out–out signal (the RI of the bio-solution) caused by the target analytes in the bio-solution. S is usually defined in term of a shift in the wavelength or the angle of incidence of the reflection dip, for a unit change in the RI ($S_\lambda = \Delta\lambda/\Delta n_{\rm w}$ (nm/RIU) or $S_\theta = \Delta\theta/\Delta n_{\rm w}$ (deg/RIU)). Thus, the reflectance of the multilayer stacks with respect to changeable RI of bio-solution is analyzed as a function of wavelength and angle that are plotted in Figs. 7(a) and 7(b). With the refractive indices of the bio-solution changing from 1.330 to 1.340 in an interval of 0.002, one can find that the reflection dip meets a red-shift, but the depths of the dips are decreased. Figure 7(b) shows that the shift of resonant angle caused by the refractive indices of the bio-solution is almost at the same interval. According to the reflectance spectrum modulated by refractive indices, the sensitivity of the biosensor is studied as shown in Figs. 7(c) and 7(d). The BSW peak is shifted by 10.4 nm on varying the RI by 0.01, demonstrating that the sensitivity S_λ reaches 1040 nm/RIU. Similarly, the sensitivity S_θ is 25.1°/RIU in the same condition, which is higher than the values reported previously.[19,20,41] Moreover, to unify the sensitivity of the two definitions, we calculated the FOM that is defined as the ratio of sensitivity to FWHM of the reflectance curve ($F = S/\text{FWHM}$). The maximum FOM is obtained in the order of magnitude 3000 RIU^{-1} in both two ways.

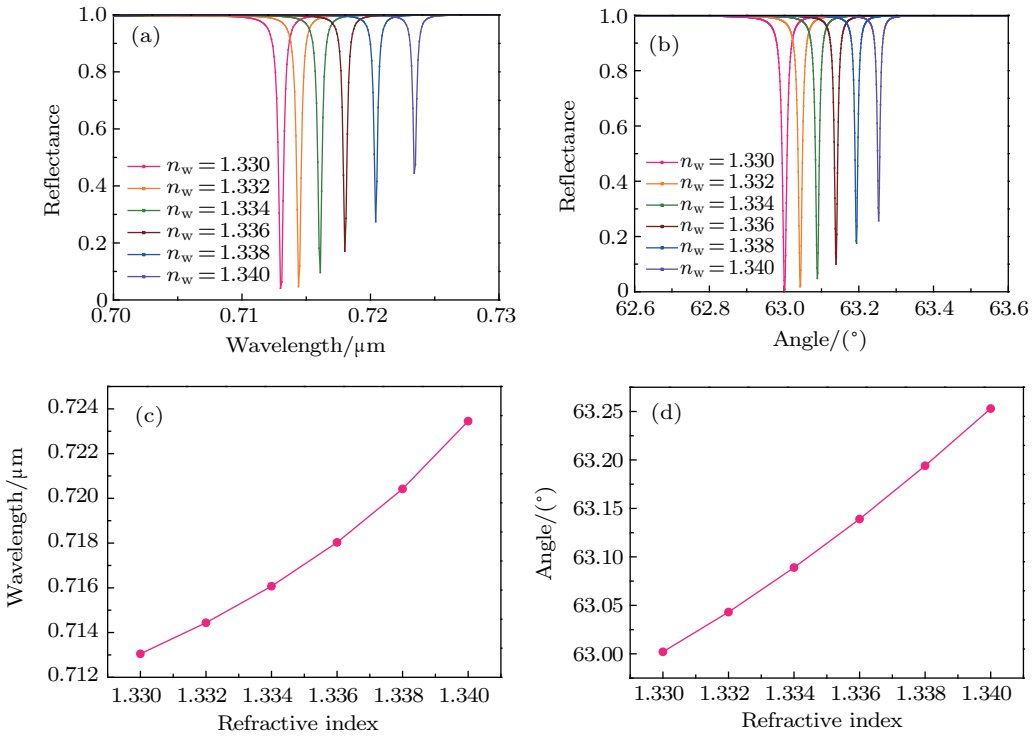


Fig. 7. (color online) (a) Variation of reflectance as a function of wavelength under different refractive indices. (b) Variation of reflectance as a function of incident angle under different refractive indices. (c) Variation of resonance wavelength with changeable RI of bio-solution. (d) Variation of resonance angle with changeable RI of bio-solution. All the structural parameters are the same as that in Fig. 2.

4. Summary

In summary, the excitation and confinement of BSWs in graphene-based 1D PhCs and its sensing applications in biomolecule detection is analyzed over a broad wavelength range. Due to the unrivaled role of graphene, BSWs can be excited and then confined effectively at the interface of PhC–solution in the process of the light–matter interaction, which is clearly illustrated by the magnetic field distribution. Furthermore, the reflectance spectra as a function of incident wavelength and incident angle are discussed in conditions of the changeable thickness of a unit cell of PhCs, numbers of graphene layers, and variable concentrations of bio-solution. Finally, in order to more accurately describe the performance of the sensor, the sensitivity and FOM of the designed sensor are studied, which finds that they are both enhanced significantly compared to SPR biosensors. Thus, the proposed configuration may provide a new window for designing high-performance optical sensors by combining the advantages of 2D materials like graphene and the latest nanofabrication techniques.

References

[1] Wang T B, Liu N H, Yu T B, Deng X H, Xu X M and Liao Q H 2014 *Chin. Phys. B* **23** 044101
[2] Yu L B, Barakat E, Francesco J D and Herzig H P 2015 *Opt. Express* **23** 31640
[3] Konopsky V N, Karakouz T, Alieva E V, Chiara V, Sekatskii S K and Giovanni D 2013 *Sensors* **13** 2566
[4] Meng Q Q, Zhao X, Chen S J, Lin C Y, Ding Y C and Chen Z Y 2017 *Chin. Phys. B* **26** 124213
[5] Liu Y C, Chen H L, Li S G, Liu Q and Li J S 2017 *Chin. Phys. B* **26** 104211
[6] Weng S J, Pei L, Wang J S, Ning T G and Li J 2016 *Chin. Opt. Lett.* **14** 110603
[7] Lan G Q, Liu S G, Zhang X R, Wang Y X and Song Y L 2016 *Chin. Opt. Lett.* **14** 022401
[8] Dubey R, Lahijani B V, Häyrinen M, Roussey M, Kuittinen M and Herzig H P 2017 *Photon. Res.* **5** 494
[9] Michelotti F, Rizzo R, Sinibaldi A, Munzert P, Wächter C and Danz N 2017 *Opt. Lett.* **42** 2798.
[10] Guo Y, Yan L, Pan W, Luo B and Luo X 2014 *Plasmonics* **9** 951
[11] Tu T Y, Pang F F, Zhu S, Cheng J J, Liu H H, Wen J X and Wang T Y 2017 *Opt. Express* **25** 9019
[12] Dubey R, Lahijani B V, Barakat E, Häyrinen M, Roussey M, Kuittinen M and Herzig H P 2016 *Opt. Lett.* **41** 4867
[13] Liscidini M and Sipe J E 2009 *J. Opt. Soc. Am. B* **26** 279
[14] Kang X B, Liu L J, Lu H, Li H D and Wang Z G 2016 *J. Opt. Soc. Am. A* **33** 997
[15] Occhicone A, Sinibaldi A, Sonntag F, Munzert P, Danz N and Michelotti F 2017 *Sens. Act. B* **247** 532
[16] Sinibaldi A, Danz N, Descrovi E, Munzert P, Schulz U, Sonntag F, Dominici L and Michelotti F 2012 *Sens. Act. B* **174** 292
[17] Sinibaldi A, Fieramosca A, Rizzo R, Anopchenko A, Danz N, Munzert P, Magistris C, Barolo C and Michelotti F 2014 *Opt. Lett.* **39** 2947
[18] Qiao H, Guan B, Gooding J J and Reece P J 2010 *Opt. Express* **18** 15174
[19] Rivolo P, Michelotti F, Frascella F, Digregorio G, Mandracci P, Dominici L, Giorgis F and Descrovi F E 2012 *Sens. Act. B* **161** 1046
[20] Li Y, Yang T, Song S, Pang Z, Du G and Han S 2013 *Appl. Phys. Lett.* **103** 04116
[21] Varghese S, Lonkar S, Singh K, Swaminathan S and Abdala A 2015 *Sens. Act. B* **218** 160
[22] Kulkarni G S, Reddy K, Zhong Z H and Fan X D 2014 *Nat. Commun.* **5** 4376
[23] Ye Z B, Tai H L, Guo R, Yuan Z, Liu C H, Su Y J, Chen Z and Jiang Y D 2017 *Appl. Surf. Sci.* **419** 84
[24] Pu M, Chen P, Wang Y, Zhao Z, Wang C, Huang C, Hu C and Luo X 2013 *Opt. Express* **21** 11618
[25] Li S, Luo J, Anwar S, Li S, Lu W, Hang Z, Lai Y, Hou B, Shen M and Wang C 2015 *Phys. Rev. B* **91** 220301
[26] Grigorenko A N, Polini M and Novoselov K S 2012 *Nat. Photon.* **6** 749
[27] Koppens F H, Chang D E and García de Abajo F J 2011 *Nano Lett.* **11** 3370
[28] Ju L, Geng B, Horng J, Girit C, Martin M, Hao Z, Bechtel H A, Liang X, Zettl A, Shen Y R and Wang F 2011 *Nat. Nanotechnol.* **6** 630
[29] Low T and Avouris P 2014 *ACS Nano* **8** 1086
[30] Schedin F, Lidorikis E, Lombardo A, Kravets V G, Geim A K, Grigorenko A N, Novoselov K S and Ferrari A C 2010 *ACS Nano* **4** 5617
[31] Bruna M and Borini S 2009 *Appl. Phys. Lett.* **94** 031901
[32] Liu J T, Liu N H, Li J, Li X J and Huang J H 2012 *Appl. Phys. Lett.* **101** 052104
[33] Merzlikin A M and Baryshev A V 2014 *Appl. Opt.* **53** 3142
[34] Yu D L, Du C Y, Shen H J, Liu J W and Wen J H 2017 *Chin. Phys. Lett.* **34** 076202
[35] Yin G, Yuan J, Jiang W, Zhu J F and Ma Y G 2016 *Chin. Phys. B* **25** 114216
[36] Zhan T, Shi X, Dai Y, Liu X and Zi J 2013 *J. Phys.: Condens. Matter* **25** 215301
[37] Deng X H, Liu J T and Yuan J R 2015 *Europhys. Lett.* **109** 27002
[38] Li X F, Peng W, Zhao Y L, Wang Q and Wei J L 2016 *Chin. Phys. B* **25** 037303
[39] Pirotta S, Xu X J, Delfan A, Mysore S, Maiti S, Dacarro G, Patrini M, Galli M and Guizzetti G 2013 *J. Phys. Chem. C* **117** 6821
[40] Sreekanth K V, Zeng S, Shang J, Yong K T and Yu T 2012 *Sci. Rep.* **2** 737
[41] Baghbadorani H K, Barvestani J and Entezar S R 2017 *Appl. Opt.* **56** 462